Sustainable Food Technology

ROYAL SOCIETY OF CHEMISTRY

PAPER

View Article Online
View Journal

Cite this: DOI: 10.1039/d6fb00103c

Fabrication of sustainable composite films based on chitosan/deep eutectic solvent/tannic acid quantum dots for bioactive pork preservation

Malin Cui, *[a] Tongtong Li, *[b] Dongmei He,[a] Miaoling Huang[a] and Shuqin Chen*[a]

Received 31st March 2026
Accepted 29th April 2026

DOI: 10.1039/d6fb00103c

rsc.li/susfoodtech

In this work, a sustainable composite film was fabricated by incorporating a citric acid/betaine-based deep eutectic solvent (DES) into a chitosan/tannic acid quantum dots (CS/TAQD) matrix. The addition of the DES increased the interfacial bonding compatibility between CS and TAQDs, and thus the tensile strength and elongation at break of the composite film were significantly improved. This composite film exhibited excellent UV barrier capacity and antioxidant capacity with a 2,2-diphenyl-1-picrylhydrazyl free radical scavenging ratio of 97.8%. It showed outstanding antibacterial performance against *Staphylococcus aureus* and *Escherichia coli*, which indicates that it can be used for pork preservation. The total volatile base nitrogen test demonstrated that the pork preservation by the CS/DES/TAQDs composite film showed a lower TVB-N value than that of a commercialized polyethylene film. The pork shelf-life can be prolonged to 7 days at 4 °C. This composite film can be completely biodegraded within 7 days in a natural environment, suggesting its great application potential in the food packaging field.

Sustainability spotlight

Conventional food packaging relies heavily on non-renewable petroleum-based plastics, resulting in serious environmental concerns. This work develops a sustainable bioactive film using renewable chitosan and tannic acid, which exhibits excellent biodegradability and enhances food preservation. By extending the shelf life of foods, this technology directly tackles food waste. From a sustainability perspective, this advancement aligns with UN SDG 12 (Responsible Consumption and Production) by offering a green alternative to petroleum-based plastics and supports SDG 13 (Climate Action) by reducing the carbon footprint associated with plastic waste.

1. Introduction

Growing environmental concerns and heightened food safety requirements have accelerated the development of biodegradable active packaging materials. Traditional petroleum-based plastics offer excellent barrier properties but are non-biodegradable, posing significant long-term threats to the ecological environment.[1] Chitosan (CS)-based polysaccharide films have gained considerable attention for their biodegradability, film-forming ability, and intrinsic antibacterial properties. Pure CS films have weak strength, high water sensitivity, and low antioxidant activity, limiting their use in advanced food packaging. To address these limitations, recent research has focused on incorporating polyphenolic compounds, nanomaterials, and green solvents into CS-based matrices to develop multifunctional composite packaging materials.[2–4]

Tannic acid (TA), a natural plant-derived polyphenol, is a promising additive due to its multiple hydroxyl groups that can form hydrogen bonds and cross-links with CS chains. As a natural antibacterial and antioxidant agent, TA can significantly enhance film performance when combined with the antimicrobial properties of CS, resulting in excellent antioxidant and antibacterial effects.[5–7] For instance, Qiu *et al.* integrated the antibacterial and antioxidant properties of both TA and CS to develop a TA/CS–citric acid (TA/CS–CA) bio-based film for effectively prolonging strawberry freshness at room temperature.[8] The cross-linking interactions between TA and CS contributed to a denser film structure, allowing for the slow and controlled release of antibacterial agents. Hou *et al.* constructed a zein/CS Janus film using a layer-by-layer casting method *via* incorporating a Pickering emulsion co-loaded with TA and cinnamon essential oil (CEO). This design enabled a sustained, unidirectional release of antibacterials *via* quasi-Fickian diffusion, achieving over 99% inhibition of key foodborne pathogens and extending pork shelf life by six days.[9] Vargas *et al.* found that the incorporation of TA facilitated the sustained release of thyme extract polyphenols within the film, effectively delaying

[a]*Key Laboratory of Chemical Materials and Green Nanotechnology, The Key Laboratory of Fujian Provincial Higher Education, College of Chemical Engineering and Materials Science, Quanzhou Normal University, Quanzhou 362000, P. R. China. E-mail: malincui@qztc.edu.cn; chenshuqin@qztc.edu.cn*

[b]*Rubber Research Institute, Chinese Academy of Tropical Agricultural Sciences, Haikou, 571101, P. R. China. E-mail: tongxinltt@163.com*

food oxidation and spoilage, and providing a new strategy for the controlled release of natural antioxidants.[10]

When TA is polymerized or incorporated in a nanostructured form, it can markedly improve the mechanical strength, hydrophobic properties, and bioactivity of the film material. Jiang *et al.* developed quaternized chitosan/TA nanoparticles (QCs/TA NPs) by combining TA with QCs through electrostatic interactions, which significantly enhanced the overall properties of K-NP films. When applied as a composite coating for banana preservation, it effectively delayed ripening, suppressed browning, and slowed oxidative deterioration.[11] The hybridization of poly(tannic acid) (PTA) with TiO_2 to form TP-NPs effectively reduced the bandgap, enhanced visible light absorption, and improved the separation efficiency of photogenerated charge carriers. As a result, the photocatalytic activity significantly increased the antibacterial ratio to 92%, maintained the desirable color and firmness of kiwifruit and delayed ripening and decay.[12] The CS-gelatin composite films modified with light-responsive Cu-TA NPs exhibited outstanding antibacterial, antioxidant, and photothermal properties, which contributed to effectively extending the shelf life of strawberries.[13]

Crosslinking agents are essential for upgrading natural polymer-based films into functional packaging materials. By constructing molecular networks, they effectively address key limitations such as poor chemical resistance, low mechanical stability, swelling, and inadequate barrier properties.[3] However, conventional crosslinkers (*e.g.*, diamines and halides) are often toxic and incompatible with the principles of green chemistry, highlighting the urgent need for eco-friendly alternatives. The DESs, as sustainable green plasticizers, can establish hydrogen-bonded networks with CS, thereby enhancing film flexibility and dynamic self-repair capacity. Furthermore, DESs can form strong hydrogen bonds or electrostatic interactions with the phenolic hydroxyl groups of polyphenols, effectively "anchoring" the polyphenols within the chitosan matrix. This anchoring restricts the migration of polyphenols, preventing their initial burst release and thereby enabling a more sustained and controllable release profile. As a non-aqueous or low-water-content medium, a DES provides a chemically stable microenvironment for polyphenols, enabling them to retain higher bioactivity upon final release. Such sustained-release behavior ensures that polyphenols are continuously released during food storage, maintaining an effective concentration within the packaging, enhancing the antioxidant and antibacterial activities of the film, and extending the shelf life of food products.[14–16] The incorporation of DES-tomato extracts into bioactive CS films significantly improved thermal stability, UV-blocking performance, and hydrophilicity. The modified composite films exhibited an approximately 1.6-fold increase in radical scavenging efficiency and a 55.41% reduction in the decay ratio of strawberries.[17] The DES composed of CA and choline chloride can form a dynamic hydrogen-bonding network with CS, significantly improving the film's flexibility and self-healing ability. This provided a promising strategy for the development of smart packaging materials.[18]

In this study, a sustainable bio-based CS/DES/TAQDs composite film was developed by incorporating a DES composed of CA and betaine, along with TAQDs, into a CS matrix. This was the first study to report the incorporation of TAQDs and DES into CS-based film systems. Although DESs have been previously used as plasticizers or modification agents for CS films, their application in simultaneously dispersing TAQDs and anchoring polyphenols within a CS matrix has not

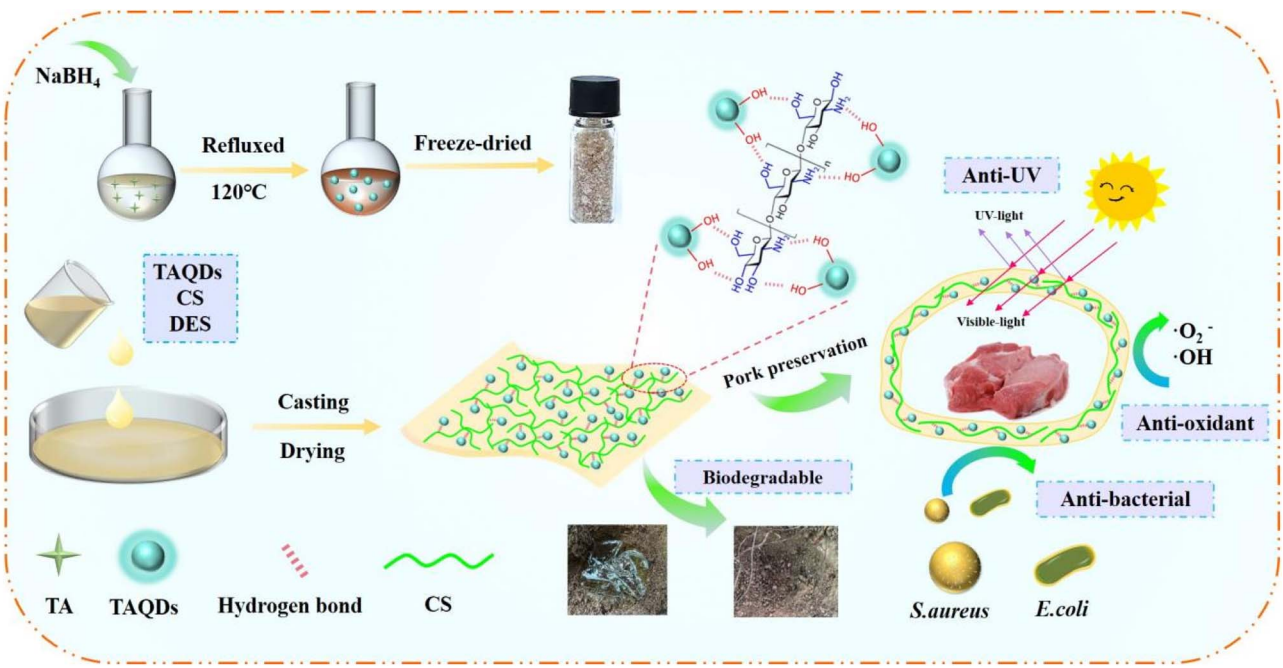

Fig. 1 Preparation of TAQDs and the CS/DES/TAQDs composite film, and the properties of the CS/DES/TAQDs composite film and its application in preservation of pork.

been explored. This CS/DES/TAQDs ternary system offered key advantages: (i) the DES promoted a denser film structure and formed strong hydrogen bonds with the phenolic hydroxyl groups of TAQDs, effectively anchoring them within the CS matrix; (ii) this anchoring restricted the initial burst release of polyphenols, enabling a more sustained and controllable release profile; (iii) the microenvironment of the DES preserved the bioactivity of TAQDs, resulting in enhanced and prolonged antioxidant and antibacterial performance compared to conventional TA/CS or other modified CS materials. This CS/DES/TAQDs composite system aimed to serve as an active packaging material for food preservation by harnessing the synergistic effects of enhanced mechanical properties, improved barrier properties, and elevated bioactivity. The structural characteristics, antioxidant and antibacterial activities, and pork preservation performance of the DES/CS/TAQDs films were systematically evaluated (Fig. 1). These findings offer a promising and scalable strategy for the development of green, efficient, and multifunctional food packaging materials, addressing both environmental sustainability and meat safety requirements.

2. Materials and methods

2.1 Materials

Chitosan (CS, $(C_6H_{11}NO_4)_n$, 500 000–1 000 000, and deacetylated 90%) was purchased from Shandong Luhai Lansheng Biotechnology Co., Ltd. Tannic acid (TA) was obtained from Shandong Yousu Chemical Technology Co., Ltd. Betaine ($C_5H_{11}NO_2$) was obtained from Shanghai Aladdin Biochemical Technology Co., Ltd. Citric acid (CA) monohydrate, sodium borohydride ($NaBH_4$), anhydrous potassium carbonate (K_2CO_3), hydrochloric acid (HCl), and anhydrous ethanol (CH_3CH_2OH) were purchased from Xilong Science Co., Ltd. Boric acid (H_3BO_3), glacial acetic acid (HAc), 2,2-diphenyl-1-picrylhydrazyl (DPPH), anhydrous sodium carbonate (Na_2CO_3), and anhydrous sodium carbonate (Na_2CO_3) were purchased from Sinopharm Chemical Reagent Co., Ltd. Nutrient agar medium was purchased from Qingdao Hope Bio-Technology Co., Ltd. *Staphylococcus aureus* (*S. aureus*) and *Escherichia coli* (*E. coli*) were obtained from the Second Affiliated Hospital of Fujian Medical University.

2.2 Preparation of the deep eutectic solvent (DES)

The DES was prepared following the procedure reported by Xia *et al.* with slight modifications.[19] Betaine and CA monohydrate were mixed with a molar ratio of 1 : 4 and stirred in an oil bath at 90 °C for 1.5 h until a transparent and viscous liquid was obtained. Subsequently, 30% (w/w) ultrapure water was added, and the mixture was continuously stirred for 0.5 h. The formed transparent and homogeneous DES was cooled to ambient temperature for use.

2.3 Preparation of tannic acid quantum dots

The TAQDs were prepared by one-pot synthesis. Specifically, 2.00 mL of 0.5 M $NaBH_4$ solution was introduced into 10.00 mL of 3 mM TA solution under continuous stirring, and this mixture was refluxed at 120 °C. After refluxing for 40 min, the solution color changed from pale yellow to orange yellow, and then turned to reddish-brown in about 2 h, suggesting the formation of a brown TAQDs solution. The TAQDs dispersion was subsequently freeze-dried to obtain a brown fluorescent TAQDs powder, which was stored at room temperature for use. The resulting TAQDs were used without further washing.

2.4 Preparation of composite films

2.4.1 Preparation of film-forming solution. The CS film-forming solution (2%, w/v) was prepared by dispersing 2.00 g CS powder into 0.2 M CA solution, followed by vigorous stirring at room temperature for 1 h until a uniform and transparent CS solution formed. Subsequently, varying amounts of DES solution (0, 0.10, 0.20, 0.30, 0.40 and 0.50 g) were incorporated into 15.00 g CS solution and completely homogenized. The resulting film-forming solutions were labeled CS, CS/DES1, CS/DES2, CS/DES3, CS/DES4, and CS/DES5.

2.4.2 Preparation of CS-based composite films. Composite films were fabricated by the casting method. Specifically, various amounts of TA powder (0.10, 0.11, 0.12, 0.13 and 0.14 g) and TAQDs powder (0.10, 0.11, 0.12, 0.13 and 0.14 g) were individually added to the CS/DES3 film-forming solution. Each mixture was stirred until a transparent and homogeneous solution was obtained, poured into 9-cm Petri dishes, and dried at 50 °C for 24 h. These films were designated as CS/DES/TA1, CS/DES/TA2, CS/DES/TA3, CS/DES/TA4, CS/DES/TA5, CS/DES/TAQDs1, CS/DES/TAQDs2, CS/DES/TAQDs3, CS/DES/TAQDs4, and CS/DES/TAQDs5, respectively.

2.5 Characterization

2.5.1 Characterization of film structures. The TAQDs microstructure was observed by high resolution transmission electron microscopy (HRTEM, FEI Talos F200S) at 200 kV. The surface and cross-section morphologies of the composite films were analyzed *via* Scanning Electron Microscopy (SEM, Hitachi S-4800). X-ray diffraction (XRD, D8 Advance, Bruker AXS Co., Ltd.) with Cu-Kα radiation (40 kV, 40 mA) was employed to determine the crystalline structure of the films over a 2θ range of 10–80°. Fourier transform infrared (FTIR) spectra were recorded on a Thermo Nicolet FTIR spectrometer. Thermogravimetric analysis (TGA, METTLER TOLEDO TG-50/MT5) was performed from 35 to 800 °C at a heating rate of 10 °C min^{-1} under a nitrogen atmosphere to evaluate the thermal stability of the films.

2.5.2 Mechanical properties. Rectangular specimens (20 mm × 70 mm) of the composite films were prepared to evaluate tensile strength (TS) and elongation at break (EB). Measurements were performed using a universal testing machine (LD24, Shenzhen Lanbo Sansi Materials Co. Ltd, China) operated at a crosshead speed of 50 mm min^{-1}. The thickness of the films was measured at five different positions using a digital micrometer (Sanliang, Japan, accuracy 0.001 mm), and the average thickness was used for calculations. All tensile tests were conducted in quintuplicate, and the average

values were reported. The TS was calculated according to the following equation:

$$\mathrm{TS} = \frac{F}{W \times B}$$

In this equation, F denotes the maximum load (N), W is the width of the film and B is the thickness of the film.

The EB(%) was calculated using the following expression:

$$\mathrm{EB}(\%) = \frac{L - L_0}{L_0} \times 100\%$$

where L_0 indicates the gauge length (mm); L denotes the distance between gauge marks at fracture (mm).

2.5.3 Water contact angle (WCA) and water solubility (WS). Composite films were cut into 10 mm × 30 mm for the WCA measurements using the sessile drop method on a JY-PHb tester (Chengde Youte Testing Instrument Co., Ltd, China). A droplet of ultrapure water was placed on the of film surface and immediately photographed. The WS of the films was assessed by dissolving 0.3 g film in 50 mL ultrapure water with continuous stirring at 1000 rpm at room temperature. The time required for complete dissolution was recorded. All measurements were conducted in triplicate, and the mean values were reported. The WS was calculated using the equation: WS = m/t, (g s^{-1}).

2.5.4 The light transmittance. The light transmittance of the films was recorded across a wavelength range of 200–800 nm using a UV-vis spectrometer (Model Specord S600, Analytik Jena AG, Germany), with air employed as the baseline reference for each measurement.

2.5.5 Antioxidant and antibacterial activities. The antioxidant activity of the films was evaluated using the 2,2-diphenyl-1-picrylhydrazyl (DPPH$^{\bullet}$) radical scavenging test. The films were dried to a constant mass at 50 °C, and 0.1 g film sample was dissolved in 1.00 mL water to obtain film solution. The 0.10 mM DPPH ethanol solution was added into film solution, vortex-mixed and incubated in the dark at room temperature for 30 min. The mixture was centrifuged at 13 000 rpm for 20 min to remove the flocculent precipitate, and the absorbance of the supernatant was recorded at 517 nm. The ultrapure water in place of the film solution served as the control. The DPPH$^{\bullet}$ scavenging activity was calculated as follows: DPPH$^{\bullet}$ scavenging activity (%) = $[(A_0 - A_s)/A_0] \times 100\%$, where A stands for the absorbance, and subscripts 0 and s denote the control and sample, respectively.

The antibacterial activity of film solution was evaluated against *S. aureus* and *E. coli* using the agar plate count method. Equal volumes of bacterial solution and film solution were mixed thoroughly. Then, the 10 μL mixture was diluted with 290 μL physiological saline to obtain a bacterial concentration of 1 × 10^6 CFU mL^{-1}. Finally, the 20 μL treated bacteria suspension was spread onto the agar plate and incubated at 37 °C for 18 h. The bacterial suspension without film solution was used as the blank. All experiments were conducted in triplicate, and the results were analyzed *via* the bacterial survival ratio.

2.5.6 Biodegradability analysis of the films under environmental conditions. To assess the biodegradation performance of CS/DES/TAQDs composite films, a soil-burial test was conducted under natural conditions. Specimens of the composite film and commercial PE film were buried side by side in the same soil plot. The degradation of both films was inspected and documented daily at the same time of day.

2.5.7 Application for pork preservation. The pork samples were wrapped with the PE film, CS/TA3 film, CS/TAQDs3 film and stored for one week. The mass was recorded every day to estimate the storage quality. The mass loss percentage was calculated as follows: mass loss ratio = $(m_0 - m_1)/m_0 \times 100\%$, where m_0 stands for the initial mass, and m_1 represents the mass stored for a specific time. Unwrapped pork was used as the blank.

Total volatile basic nitrogen (TVB-N) was determined by the micro-diffusion method in accordance with the National Food Safety Standard (GB 5009.228-2016) to assess the storage quality of pork samples. The pork was minced using a meat grinder, and 20 g mince was dispersed in 100 mL water in a capped conical flask. The suspension was left to stand for 30 min, and then filtered. The filtrate was stored at 4 °C until analysis. The H_3BO_3 solution (1 mL, 20 g L^{-1}) and one drop of the mixed indicator (1 g L^{-1} methyl red ethanol solution and 1 g L^{-1} bromocresol green ethanol solution, v/v = 1 : 5) were added into the center of the diffusion dish. Water-soluble adhesive was evenly applied to the edge of the diffusion dish. 1.0 mL of filtrate and 1.0 mL saturated K_2CO_3 solution were quickly dispensed into the outer chamber, the frosted glass lid was placed flat to seal, and the dish was gently rotated to thoroughly mix the sample with K_2CO_3. It was incubated at 37 °C for 2 h and then cooled to room temperature.

0.0100 M HCl and mixed indicator were used to titrate H_3BO_3 solution, and the endpoint was indicated by a purplish-red color. Fresh pork was used as the blank for the TVB-N determination.

The TVB-N was calculated according to the following equation:

$$X = \frac{(V_1 - V_2) \times c \times 14}{m \times (V/V_0)} \times 100$$

where X is the TVB-N content with the unit of mg per 100 mL; V_1 and V_2 are the volumes of the HCl standard titrant consumed by the test solution and reagent blank, respectively; c is the concentration of HCl standard titration solution; 14 is the molar mass of the N element; m is the weight of the pork sample; V is the filtrate volume; V_0 is the total volume of sample solution; 100 is the conversion coefficient. TVB-N in pork was calculated as the arithmetic mean of two independent determinations performed under repeatability conditions.

3. Results and discussion

3.1 Preparation of TAQDs and composite films

The TAQDs were prepared by one-pot synthesis. In the synthesis of TAQDs, $NaBH_4$ played a subtle and multifaceted role. Upon rapid hydrolysis in water, $NaBH_4$ generated a large quantity of OH^- ions, creating a strongly alkaline environment. This alkaline environment activated the phenolic hydroxyl groups of TA,

rendering them more susceptible to oxidation, thereby efficiently initiating an oxidative self-polymerization reaction to form polytannic acid (PTA) oligomers. Under sustained alkaline conditions and reflux at elevated temperature, these PTA nanoparticles underwent further dehydration, cyclization, and partial carbonization, resulting in the formation of fluorescent TAQDs. Concurrently, the reducing capability of $NaBH_4$ can reduce partially over-oxidized intermediates, preventing the complete oxidative degradation of TA. This dual action enabled precise control over the degree of crosslinking and carbonization, ensuring the formation of structurally well-defined and stable nanoparticles instead of amorphous precipitates.

TEM revealed that the TAQDs were uniform and well dispersed, with an average particle diameter of 1.8 nm based on statistical analysis of 200 particles (Fig. 2A and B). As shown in Fig. 2C, the sharp peaks at 1708 cm^{-1} and 1611 cm^{-1} were associated with the carbonyl group C=O stretching from aromatic esters of TA, and the peak at 1205 cm^{-1} was assigned to the C–O stretching. The peak at 3600–3000 cm^{-1} corresponds to the stretching vibration of O–H bonds from phenolic hydroxyl groups. The C=O stretching at 1611 cm^{-1} was red-shifted to 1621 cm^{-1}, and the stretching vibration of O–H bonds was weakened, which indicated that TAQDs formed through hydrogen bonding interaction.[20–23] The TAQDs displayed a broad absorption band at approximately 450 nm for the quantum confinement effects and emitted bright cyan fluorescence at 525 nm under 468 nm excitation (Fig. 2D). The CS/DES/TAQDs composite film exhibited uniformly transparent pale yellow under visible light and vivid blue emission under 365 nm UV light, attributable to the incorporated TAQDs powder (Fig. 2E and F). The observed strong fluorescence in the film indicated its potential for future application in intelligent packaging, including traceability and anti-counterfeiting, although the fluorescent properties of TAQDs were not utilized for anti-counterfeiting and product labeling in this study.

3.2 Microstructural analysis of the films

The surface and cross-sectional SEM images of the CS, CS/DES, CS/DES/TA, and CS/DES/TAQDs composite films are shown in Fig. 3. As seen in Fig. 3A and B, the CS substrate exhibited fine surface cracks and a relatively smooth cross-section. The covalently crosslinked CS film was formed through a combination of electrostatic interactions, hydrogen bonding, and hydrophobic interactions between CS molecules and CA molecules, which collectively improved the compatibility of the film's internal components.[24–26] After introducing the DES, the surface cracks were markedly reduced, a highly wrinkled surface emerged, and the cross-section displayed a distinct layered structure (Fig. 3C and D). The emergence of surface wrinkles and a laminated cross-section was attributed to DES-induced swelling of CS chains, which facilitated the formation of a strong hydrogen-bonding network within the CS matrix; this was consistent with the cross-linking and plasticizing roles of the DES.[19,27]

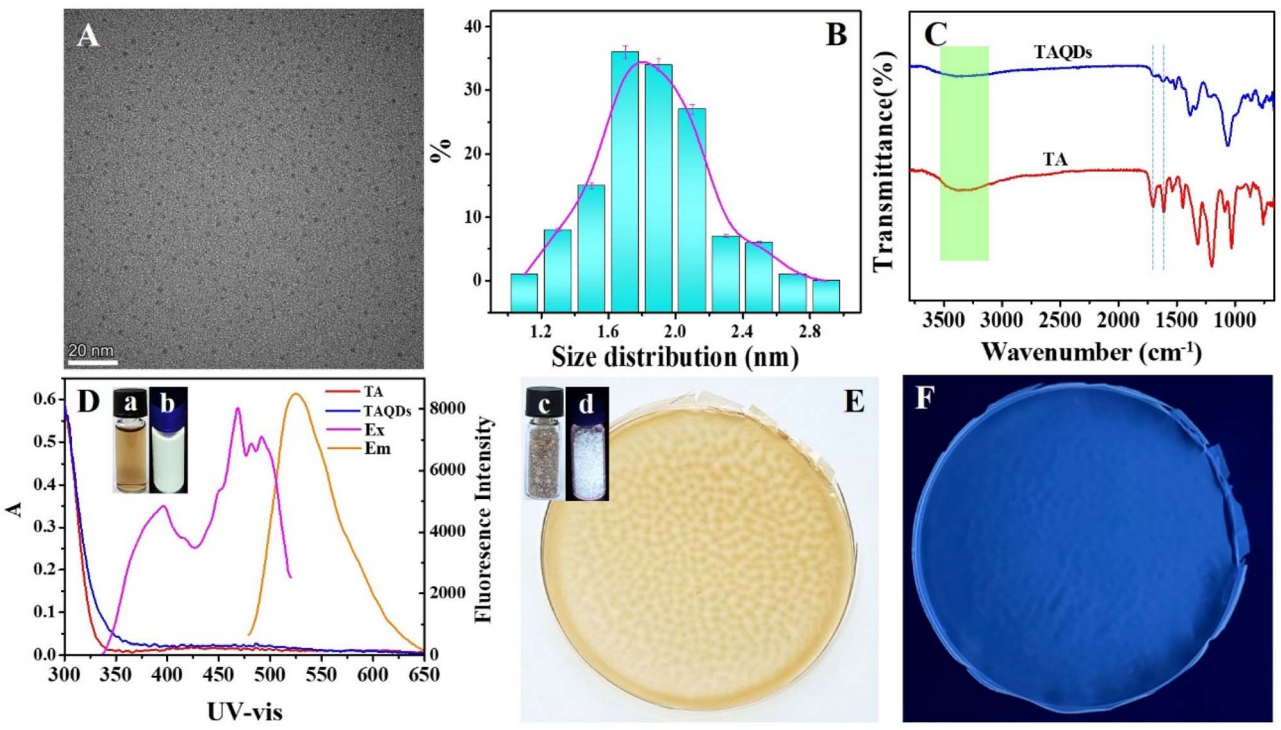

Fig. 2 (A) The TEM image of TAQDs, (B) size distribution analysis of the TAQDs from 200 random nanoparticles, (C) FTIR of TA and TAQDs, (D) UV-vis absorbance spectra of TA and TAQDs, and the fluorescence spectra of TAQDs, the inset shows the photos of TAQDs solution under visible light (a) and 365 nm UV light (b), (E) the image of the CS/DES/TAQDs composite film under visible light; the inset shows the photos of TAQDs powder under visible light (c) and 365 nm UV light (d). (F) The image of the CS/DES/TAQDs3 composite film under 365 nm UV light.

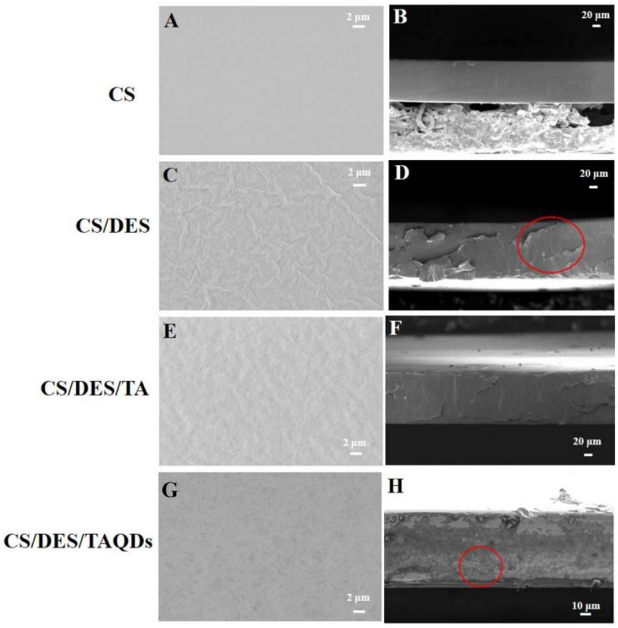

Fig. 3 SEM images of the surfaces of (A) CS, (C) CS/DES, (E) CS/DES/TA and (G) CS/DES/TAQDs films, and the cross-sections of (B) CS, (D) CS/DES, (F) CS/DES/TA and (H) CS/DES/TAQDs films.

Incorporation of TA, or TAQDs powder further diminished surface cracking, yielding a denser film surface (Fig. 3E and J). Compared with the CS/DES film, the CS/DES/TA film showed a less pronounced lamellar structure in the cross-section (Fig. 3F). By contrast, the cross-sections of the CS/DES/TAQDs film became rougher with discernible particles, indicating effective embedding of TAQDs within the CS/DES matrix (Fig. 3F and H).

3.3 Optical, thermal, and mechanical properties of the films

Fig. 4A shows the color and appearance of CS and CS/DES-based nanocomposite films. The CS, CS/DES, and CS/DES/TA films were transparent. Upon the addition of TAQDs powder, the films became pale-yellow yet remained transparent. The underlying markings remained clearly visible, indicating excellent optical clarity. The UV-vis transmittance spectra showed 0% transmittance between 200 and 330 nm. In the 330–380 nm range, the transmittance gradually decreased with increasing TA content, falling from 34.3% to 14.3%. Owing to the UV-absorbing chromophores in TA, such as phenolic hydroxyl and carbonyl groups, the CS/DES/TA film exhibited outstanding UV-shielding performance.[28–30] With the addition of TAQDs powder, the transmittance decreased to 2.2% for the CS/DES/TAQDs film, which is markedly lower than that of the CS/DES/TA film and indicates superior UV-shielding performance. On the one hand, the increased specific surface area of TAQDs provided more active sites for UV absorption. On the other hand, TAQDs significantly enhanced UV reflectance and scattering, thereby reducing UV penetration through the film. These results demonstrated that the incorporation of TAQDs significantly strengthened the UV-shielding capability of the composite films, effectively preventing UV-induced discoloration and nutrient loss in photosensitive foods (Fig. 4B and C). As shown in Fig. 4D and E, the CS/TA and CS/TAQDs films exhibited strong absorbance in the 300–400 nm range, indicating excellent UV-blocking capabilities, which mitigated photo-oxidation and light-induced damage and thus slowed food oxidation and spoilage.

The optical properties of food packaging films can significantly influence light transmittance, product display, and marketing effectiveness. Table 1 revealed the thickness and colorimetric parameters of CS and CS matrix nanocomposite films. With the addition of TA and TAQDs, the film thickness gradually increased, and the L^* value decreased slightly, indicating a modest reduction in brightness. The a^* values for CS, CS/DES, and CS/DES/TA films were −0.53, −0.33, and −0.52, respectively, confirming a slight greenish cast. Upon incorporation of TAQDs, the b^* value of the CS/DES/TAQDs rose to 7.59, indicating a more pronounced yellow hue. This warm yellow tone may enhance shelf appeal by drawing consumer attention. The total color difference (ΔE) rose from 1.53 to 9.52, reflecting a perceptible color shift and modest decline in transparency due to absorption/scattering from TAQDs.

The XRD patterns of CS, CS/DES, CS/DES/TA, and CS/DES/TAQDs film samples are shown in Fig. 5A. The broad diffraction peak at 18.3° was attributed to the allomorphic crystalline lattice of CS.[31,32] The diffraction peaks at 18.3° and 26.5° decreased for the CS/DES film, whereas the characteristic CS peaks nearly disappeared after the addition of TA or TAQDs. As a low molecular-weight plasticizer, the DES can increase the interchain spacing of CS and improve chain flexibility. Meanwhile, TA and TAQDs disrupt CS chain ordering, resulting in reduced crystallinity.

The FTIR spectra of CS, CS/DES, CS/DES/TA, and CS/DES/TAQDs films are shown in Fig. 5B. The bands at 1715 cm^{-1} and 1616 cm^{-1} were assigned to the C=O stretching vibration of COOH groups in tri-carboxylic acids and the C–O stretching vibration.[33–36] The bands at 1393 cm^{-1} and 1200 cm^{-1} were attributed to the symmetrical stretching vibration of COO– groups and the stretching vibration of the C–O–C bond, and they red shifted to 1400 cm^{-1} and 1216 cm^{-1} in the CS/DES/TAQDs film, suggesting intermolecular interactions between CS with TAQDs.

Thermogravimetric analysis (TGA) was performed to evaluate the thermal stability of CS/TA and CS/TAQDs films (Fig. 5C). All samples display a three-stage thermal degradation profile. The first stage, occurring below 165 °C, was mainly attributed to the evaporation of moisture. The second stage, ranging from 250 °C to 390 °C, corresponded to deacetylation of CS together with decomposition of the DES. The third stage, between 550 °C and 700 °C, showed a comparatively slow mass loss from oxidation of carbonized residues and further decomposition of residual $–NH_2$ and –OH functionalities in the composites. The CS/TAQDs composite film exhibited the highest thermal stability, as evidenced by delayed degradation temperatures and a reduced mass-loss ratio. The TA is rich in phenolic hydroxyl groups, while CS contains $–NH_2$ and –OH groups along its molecular chains. These functional groups can

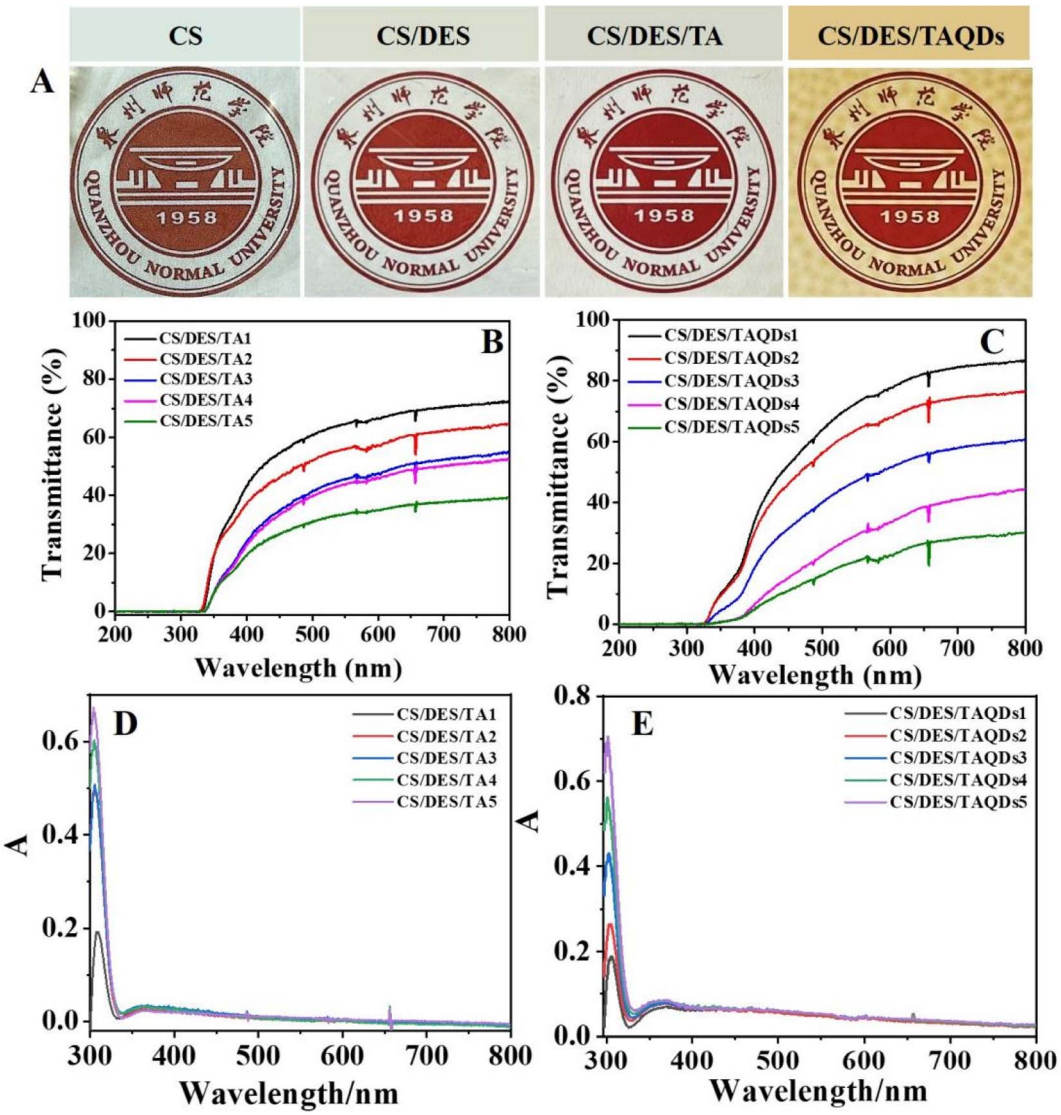

Fig. 4 (A) Photos of CS, CS/DES, CS/DES/TA, and CS/DES/TAQDs films. (B and C) Transmittance of CS/DES/TA and CS/DES/TAQDs films with different addition amounts of TA and TAQDs. (D and E) The UV-vis spectra of CS/DES/TA and CS/DES/TAQDs films.

Table 1 Thickness and surface color parameters of CS and CS-based nanocomposite films[a]

Film	Thickness (mm)	L^*	a^*	b^*	ΔE
CS	0.101 ± 0.006^{b}	24.58 ± 0.04^{b}	-0.53 ± 0.02^{d}	0.64 ± 0.01^{e}	1.53 ± 0.02^{e}
CS/DES	0.130 ± 0.004^{a}	27.25 ± 0.05^{a}	-0.33 ± 0.01^{c}	0.88 ± 0.02^{d}	3.97 ± 0.05^{c}
CS/DES/TA	0.124 ± 0.016^{a}	24.09 ± 0.02^{c}	-0.52 ± 0.02^{d}	1.61 ± 0.01^{c}	2.10 ± 0.02^{d}
CS/DES/TAQDs	0.136 ± 0.011^{a}	23.26 ± 0.02^{d}	0.56 ± 0.02^{a}	7.59 ± 0.04^{b}	7.96 ± 0.06^{b}

[a] [a–e] indicated statistically significant differences in film samples at different levels ($P < 0.05$).

form stronger intermolecular interactions such as hydrogen bonding and electrostatic interactions, which densify the molecular network, restrict chain mobility, and thereby retard thermal decomposition.[37–39]

The hydrophobicity of the CS/DES/TA and CS/DES/TAQDs films was evaluated by WCA measurements (Fig. 5D). As the concentrations of TA or TAQDs increased, the WCA values rose accordingly. This was attributed to the incorporation of TA and TAQDs, which altered the microstructure and surface morphology of the films, lowered the surface free energy and hindered water penetration, resulting in an increase in surface hydrophobicity. The CS/DES/TAQDs film exhibited the highest hydrophobicity. The aromatic rings in TA functioned as hydrophobic moieties that assemble into hydrophobic

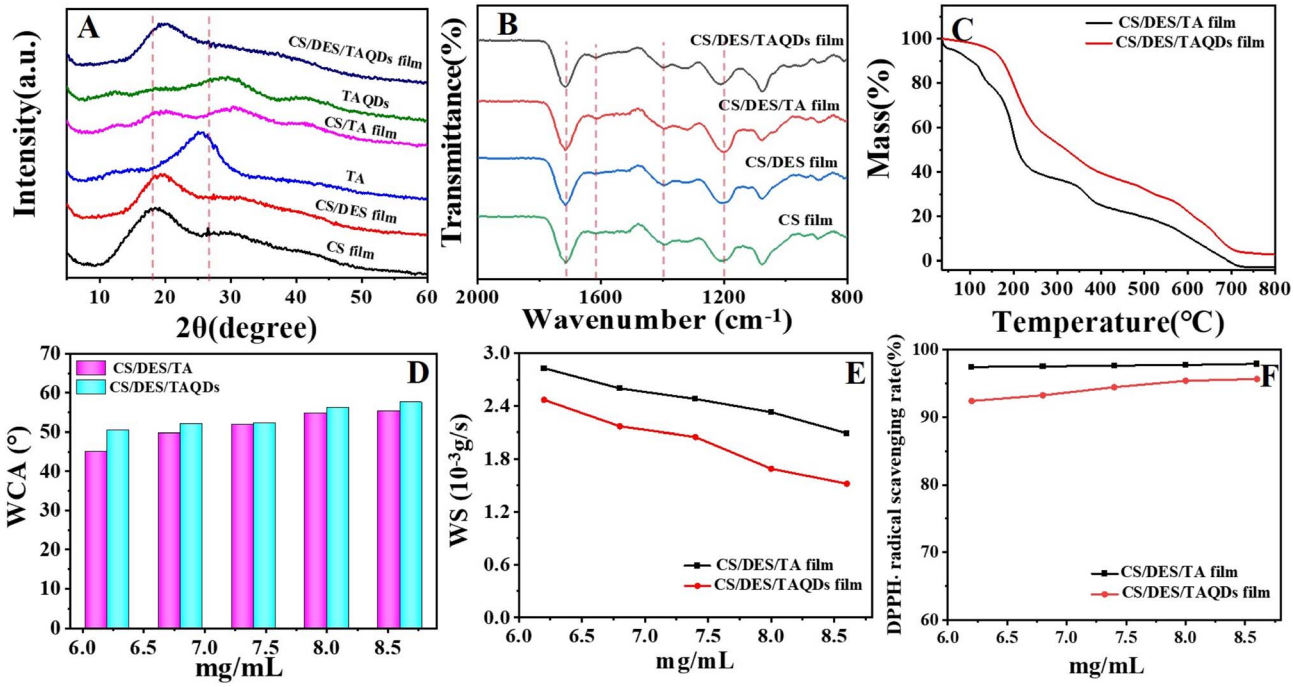

Fig. 5 (A) XRD spectra and (B) FTIR spectra of CS, CS/DES, CS/DES/TA and CS/DES/TAQDs films. (C) TGA curves, (D) WS curves, (E) WCA and (F) DPPH• scavenging rates of CS/DES/TA and CS/DES/TAQDs films.

microdomains within the film matrix, thereby decreasing overall hydrophilicity. The formation of a denser three-dimensional network reduced the effective pore size available for water transport, further enhancing water resistance.[40,41] SEM analysis also revealed that TAQDs incorporation generated micro/nanoscale protrusions on the film surface, increasing surface roughness and supporting the higher WCA. According to the Wenzel and Cassie–Baxter models, such surface roughness can trap air pockets and create a composite solid–air interface, thereby increasing the apparent WCA and hydrophobic behavior.[42–44] Improved surface hydrophobicity suppresses moisture ingress and migration, thereby prolonging the shelf life of food products. The WS of CS/DES/TA and CS/DES/TAQDs films progressively decreased with the increasing TA and TAQDs contents (Fig. 5E). This was attributed to a synergistic action of three mechanisms involving chemical crosslinking, physical barrier formation, and the introduction of hydrophobic groups, which collectively lowered the surface free energy of the films.

The antioxidant capacity of food-preservation films is pivotal, as it delays oxidation and spoilage, preserves nutritional quality, prolongs shelf life, and safeguards food safety. The antioxidant performance of CS/DES/TA and CS/DES/TAQDs films was evaluated by DPPH• radical-scavenging assays (Fig. 5F). The DPPH• scavenging ratio increased progressively with higher TA and TAQDs loadings. The CS/DES/TA exhibited the strongest antioxidant activity, with a scavenging ratio reaching 97.93%. The CS/DES/TAQDs showed a slightly lower value of 95.68%. This pronounced antioxidant behavior primarily derives from the synergy between the polyphenolic framework of TA and the polysaccharide matrix of CS. Phenolic-OH can directly capture free radicals (such as •OH, O_2^-, and ROO•) *via* hydrogen atom transfer or single electron transfer, thereby interrupting the oxidative chain reaction.[39,40,45] Under acidic conditions, protonated $-NH_3^+$ on CS engages in charge-transfer interactions with the phenolic-OH of TA, which facilitates hydrogen donation from phenolic sites and enhances scavenging efficiency. The hydrophobicity of CS/DES/TAQDs was higher than that of CS/TA, and the surface area of TAQDs was larger than that of TA molecules, leading to fewer interactions with DPPH molecules and a lower DPPH scavenging ratio than that of CS/TA. Overall, the CS/DES/TA and CS/DES/TAQDs films all exhibited excellent antioxidant properties and high research value for applications in food preservation.

As shown in Fig. 6, the incorporation of TA significantly enhanced the mechanical properties of CS-based composite films, with both TS and EB initially increasing and then decreasing as the TA content increased. When the concentration of TA or TAQDs powder reached 7.4 mg mL^{-1}, the film exhibited the highest TS and maximum EB. Notably, the CS/DES/TA film outperformed the CS/DES/TAQDs film in stress–strain performance. The CS/DES/TA3 film achieved a TS of 7.19 MPa and an EB of 72%, significantly higher than those of CS/DES/TAQDs3.

The phenolic-OH in TA molecules can interact with the $-NH_2$ of CS through hydrogen bonding and electrostatic interactions, forming a dynamic cross-linked network. This network effectively restricted CS chain mobility, thereby improving the film rigidity and toughness, and enhancing both TS and EB. However, excessive TA can lead to molecular self-aggregation and local agglomerates, which disrupt network uniformity and impeded chain mobility, ultimately degrading mechanical

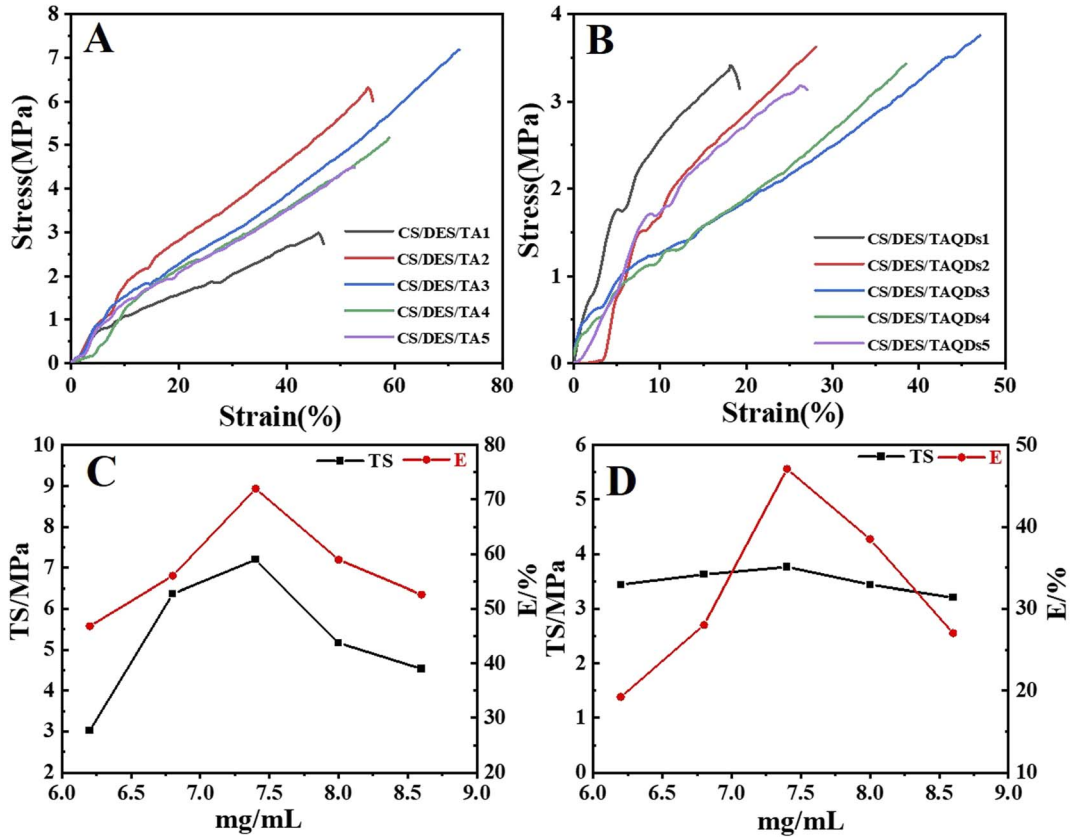

Fig. 6 The strain–stress diagram of CS/DES/TA (A) and CS/DES/TAQDs (B) films; the TS and E curve diagram of CS/DES/TA (C) and CS/DES/TAQDs (D) films with different addition amounts of TA and TAQDs powder.

performance.[46–49] By contrast, TAQDs, due to their relatively large particle size, interacted with CS primarily at the surface or in localized regions, resulting in a smaller interfacial bonding area and limited reinforcement effect.[12]

3.4 Antibacterial activity and biodegradability analysis of the films

As shown in Fig. 7, the antibacterial performance of the composite films was assessed using flat plate coating assays. Compared to the CS, CS/DES3, CS/DES/TA3 and CS/DES/TAQDs3 films, the CS/DES/TAQDs3 film demonstrated superior antibacterial performance against *S. aureus* (99.41%) and (*E. coli* 95.78%) (Table 2). The CS combined with the DES and TA formed an "electrostatic adsorption network", effectively enhancing the adsorption and immobilization of negatively charged microorganisms. TA, a natural polyphenolic compound with broad-spectrum antibacterial activity, can insert into the lipid bilayer of the cell membrane through hydrophobic interactions, increasing membrane permeability and disrupting the bacterial membrane structure. Additionally, it mitigated

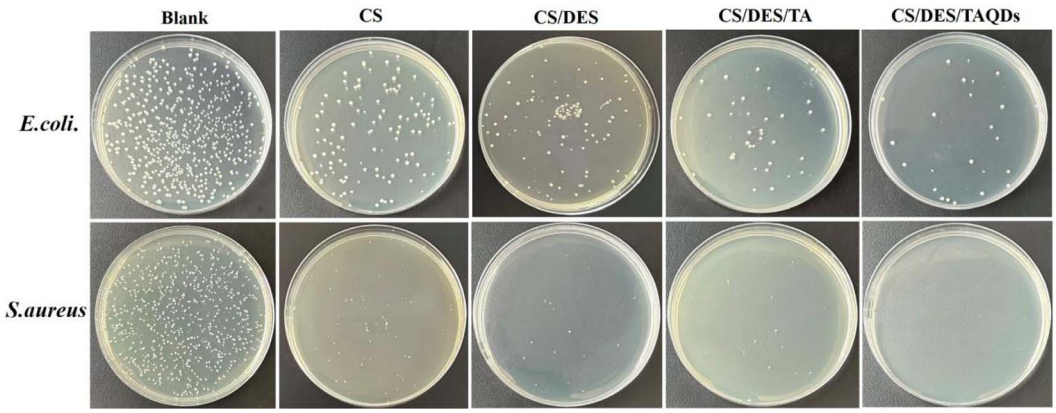

Fig. 7 Flat plate coating results of *E. coli* and *S. aureus*.

Table 2 Colony reduction rate of CS, CS/DES3, CS/DES/TA3, and CS/DES/TAQDs3 against *E. coli* and *S. aureus*

		Blank	CS	CS/DES	CS/DES/TA	CS/DES/TAQDs
E. coli	Colony count	569	161	123	42	24
	Colony reduction rate/%	—	71.10	78.38	92.62	95.78
S. aureus	Colony count	677	67	24	21	4
	Colony reduction rate/%	—	90.10	96.01	96.90	99.41

oxidative stress by scavenging free radicals generated by bacteria, thereby inhibiting bacterial proliferation.[9,50]

The TAQDs, acting as functional nanofillers, were embedded within the CS matrix to create a nanoscale porous network and high-density antibacterial sites, promoting the directional diffusion of antibacterial agents. Upon bacterial contact with the film surface, the pathogens were instantly surrounded by multiple TAQDs, increasing the likelihood of phenolic-OH attack on the bacterial membrane by more than tenfold.[50] The TAQDs enable the sustained release of TA, prolonging antibacterial efficacy and overcoming the rapid diffusion and short-lived activity typically associated with free TA.

As shown in Fig. 8, the degradation behaviors of a commercial PE cling film and CS/DES/TA3 and CS/DES/TAQDs3 films were evaluated under natural environmental conditions. The CS/DES/TA3 and CS/DES/TAQDs3 films completely decomposed within 7 days, which was driven by a synergistic action of chemical oxidation, hydrolysis, and microbial enzymatic activity. These composited films were bio-based and environmentally friendly. As bio-based and environmentally benign materials, these composite films readily break down when exposed to sunlight (UV radiation), moisture, wind, and ambient microorganisms.

In the initial stage, environmental moisture infiltrated the film and induced swelling, which initiated hydrolysis of CS chains and photo-oxidation of TA, progressively disrupting the internal network. In the intermediate stage, microorganisms colonized the film surface and secreted enzymes, gradually degrading CS and TA into small molecular intermediates. In the final stage, these intermediates were fully mineralized to CO_2, H_2O, and inorganic salts, yielding high environmental compatibility. By contrast, traditional petroleum-based cling films, composed of long-chain synthetic polymers, were highly resistant to degradation under natural conditions. Overall, the CS/DES/TA3 and CS/DES/TAQDs3 composite films exhibited outstanding biodegradability and represented a promising alternative to conventional plastic films.

3.5 Application for pork preservation

The preservation performance of a commercial PE cling film and CS/DES/TA3 and CS/DES/TAQDs3 composite films was evaluated by storing pork samples for 7 days (Fig. 9A). Sensory observations indicated that signs of spoilage and the emergence of unpleasant odors first appeared on day 4 in the blank and the group wrapped with the commercial PE cling film. The pork samples wrapped with the composite films did not exhibit noticeable spoilage odors until day 6. By day 7, the pork in the blank and PE groups exhibited overt spoilage, accompanied by fluid exudation and a pronounced putrid smell. Although fluid exudation was also observed in the samples preserved with the composite films, the odor intensity was markedly lower. The unpleasant odor primarily arises from volatile amines and sulfur compounds produced by microbial metabolism, along with aldehydes and ketones generated from lipid oxidation. TA can effectively scavenge free radicals formed during lipid oxidation, thereby delaying rancidity and suppressing odor development.

As shown in Fig. 9B, the pork in the blank group exhibited the highest weight loss during storage. The pork wrapped with

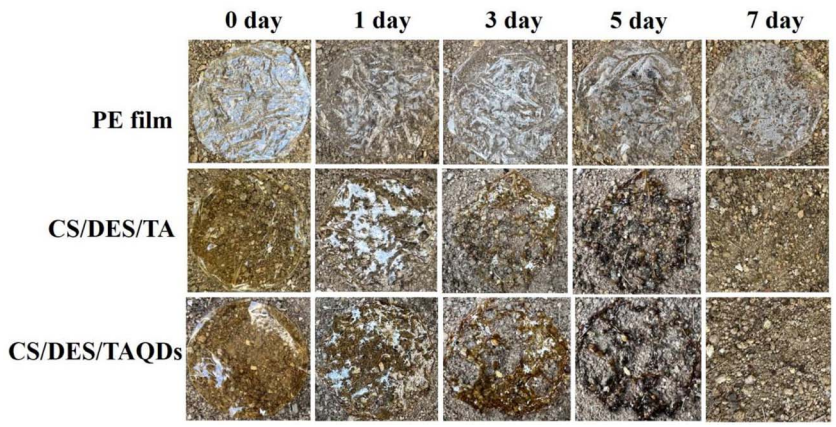

Fig. 8 The biodegradation performance of the PE cling film and CS/DES/TA3 and CS/DES/TAQDs3 composite films under natural environmental conditions.

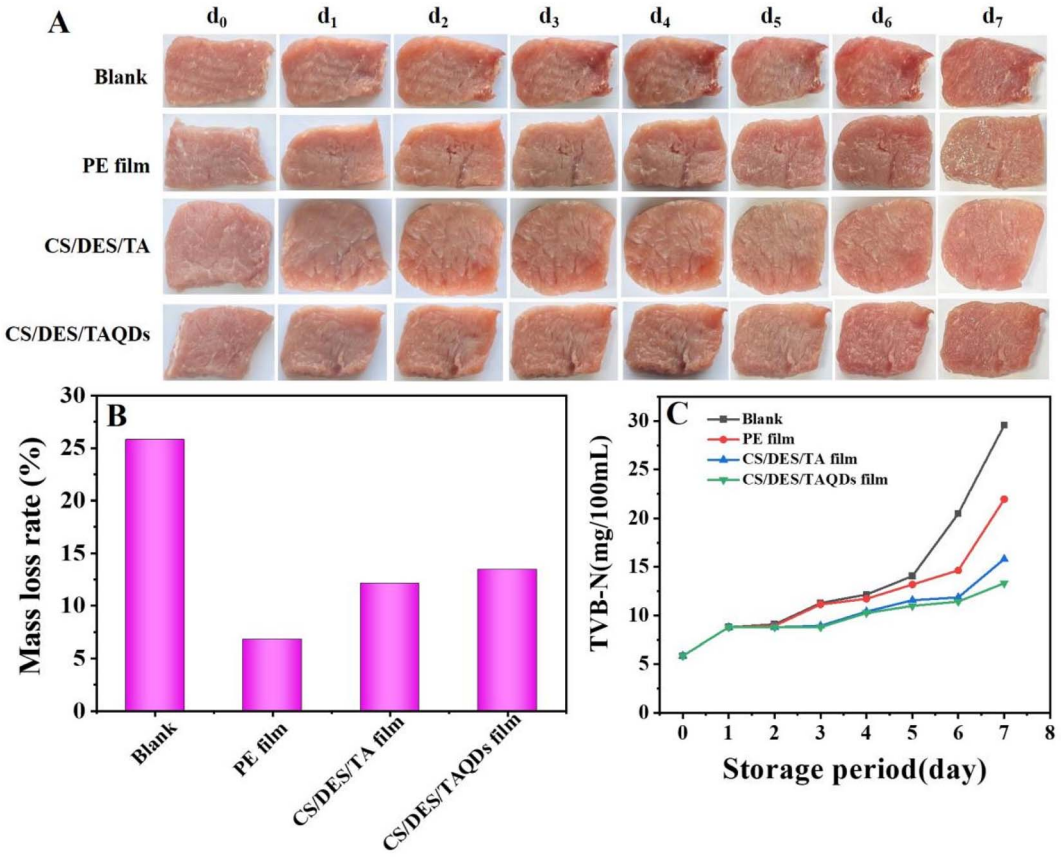

Fig. 9 (A) Pork appearance changed over storage (0–7 days) for each group, (B) pork weight loss rate, and (C) the TVB-N content change of pork.

the commercial PE cling film showed the least weight loss, followed by the CS/DES/TA3 and CS/DES/TAQDs3 groups with only a minimal difference. Fig. 9C reveals that the TVB-N content increased progressively with storage time. By day 7, the TVB-N levels ranked as follows: blank > commercial PE cling film > CS/DES/TA3 > CS/DES/TAQDs3. Notably, all three composite film groups exhibited significantly lower TVB-N levels than the blank and commercial PE cling film groups. According to national food safety standards (maximum allowable TVB-N for meat products ≤15 mg/100 mL), the pork wrapped with CS/DES/TAQDs3 films remained within the acceptable range throughout storage, indicating the effectiveness of the films in retaining meat freshness.

The commercial PE cling film relied solely on the physical barrier, had poor breathability, and lacked intrinsic antibacterial functionality. Although it can effectively block external microbial contamination, moisture and volatile amine generated by pork metabolism tend to accumulate inside the package. This created a high-humidity nutrient-rich microenvironment that accelerated rapid bacterial proliferation. By contrast, the composite films can modulate their microporous structure *via* intermolecular cross-linking, thereby forming selectively permeable films. These films not only prevented the ingress of external microorganisms but also allowed the gradual release of water vapor and metabolic gases, helping to maintain a low-humidity internal environment. With dual antibacterial and antioxidant functionalities, combined with the sustained-release behavior of embedded TAQDs and improved breathability, the composite films effectively reduced surface moisture loss, significantly delayed spoilage, and preserved the freshness and tenderness of the pork.

4. Conclusions

A sustainable and biodegradable CS/DES/TAQDs composite film was successfully fabricated using a DES-assisted method. The DES promoted the formation of hydrogen bonds and electrostatic interactions between CS and TAQDs, thereby enhancing the internal network structure of the composite film. This compact network structure effectively distributed stress, improving the film's tensile strength and flexibility. The presence of TAQDs generated micro/nano-scale protrusions on the film surface, increasing the WCA and enhancing water resistance. Rich in phenolic-OH groups, TAQDs endowed the film with strong antioxidant and antibacterial properties, achieving inhibition ratios of 99.41% against *S. aureus* and 95.78% against *E. coli*, respectively. The film degraded completely within 7 days under natural conditions, confirming excellent biodegradability. Applied to pork packaging, the film effectively suppressed microbial growth and extended shelf life by two days compared to the commercial PE film. These results highlight its significant potential for food preservation applications.

Author contributions

Malin Cui: data curation, writing – original draft preparation, methodology, investigation, funding acquisition. Tongtong Li: methodology, software. Dongmei He: visualization, investigation. Miaoling Huang: visualization, investigation. Shuqin Chen: investigation, funding acquisition. All authors have read and agreed to the published version of the manuscript.

Conflicts of interest

The authors declare that they have no known competing financial interests or personal relationships that could have appeared to influence the work reported in this paper.

Data availability

The data that support the findings of this study are available from the corresponding author upon reasonable request.

Acknowledgements

This work was supported by the Fujian Provincial Natural Science Foundation of China (Grant No. 2024J01787 and 2021J05181) and the Quanzhou City Science & Technology Program of China (2021C023R).

References

1 X. X. Huang, J. Yang, R. Huang, T. Sun, L. Yang and Z. J. Wu, Poly(vinyl alcohol)-based composite film with integrated sustainability, biodegradability, and multifunctional properties, *ACS Appl. Polym. Mater.*, 2026, **8**, 442–453, DOI: 10.1021/acsapm.5c03891.

2 Z. Y. Chang, Q. Xu, S. K. Yan, Y. L. Liu, F. L. Geng, S. G. Yuan, X. Yao, N. Ma, K. Wang, G. Y. Song and J. X. Jiang, Film based on chitosan and wood vinegar with superior antioxidant, UV-shielding, and bacteriostatic properties for food packaging, *Food Hydrocolloids*, 2025, **167**, 111430, DOI: 10.1016/j.foodhyd.2025.111430.

3 W. L. Liu, S. Kang, Q. S. Zhang, S. Chen, Q. Yang and B. Yan, Self-assembly fabrication of chitosan-tannic acid/MXene composite film with excellent antibacterial and antioxidant properties for fruit preservation, *Food Chem.*, 2023, **410**, 135405, DOI: 10.1016/j.foodchem.2023.135405.

4 Y. Mao, M. L. Cui, X. Y. Zhang, H. T. Lin and D. P. Yang, Integrating L-cysteine coated polydopamine nanoparticles and deep eutectic solvents into chitosan matrix for multifunctional food packaging application, *Chem. Eng. J.*, 2024, **498**, 155156, DOI: 10.1016/j.cej.2024.155156.

5 C. Y. He, L. B. Yuan, S. W. Bi, C. M. Zhou, Q. Yang, J. Gu, B. Yan and J. He, Modified chitosan-based coating/packaging composites with enhanced antibacterial, antioxidant, and UV-resistant properties for fresh food preservation, *ACS Appl. Mater. Interfaces*, 2024, **16**(36), 48352–48362, DOI: 10.1021/acsami.4c10643.

6 S. J. Li, X. L. Liu, X. Q. Zhang, L. L. Fan, F. Wang, J. Z. Zhou and H. Z. Zhang, Preparation and characterization of zein-tannic acid nanoparticles/chitosan composite films and application in the preservation of sugar oranges, *Food Chem.*, 2024, **437**, 137673, DOI: 10.1016/j.foodchem.2023.137673.

7 H. Fu, R. P. Huang, J. F. Li, Z. H. Lin, F. X. Wei and B. F. Lin, Multifunctional cinnamaldehyde-tannic acid nanoemulsion/chitosan composite film for mushroom preservation, *Food Hydrocolloids*, 2023, **145**, 109111, DOI: 10.1016/j.foodhyd.2023.109111.

8 L. Y. Chang, L. J. Xu, Z. W. Yang, L. B. Liu and D. Qiu, Antibacterial and antioxidative biogenic films for room-temperature strawberry preservation, *Food Chem.*, 2023, **405**, 134893, DOI: 10.1016/j.foodchem.2022.134893.

9 S. M. Fan, Q. F. Yang, C. Q. Zhu, X. Li, A. Richel, M. L. Fauconnier, F. Fang, D. Q. Zhang and C. L. Hou, Zein/chitosan Janus film incorporated with tannic acid and cinnamon essential oil co-loaded Pickering emulsion for sustained controlled release and pork preservation, *Int. J. Biol. Macromol.*, 2025, **286**, 138429, DOI: 10.1016/j.ijbiomac.2024.138429.

10 E. Talón, K. T. Trifkovic, M. Vargas, A. Chiralt and G. M. Chelo, Release of polyphenols from starch-chitosan based films containing thyme extract, *Carbohydr. Polym.*, 2017, **175**, 122–130, DOI: 10.1016/j.carbpol.2017.07.067.

11 P. P. Deng, Z. H. Wang, J. J. Bu, Y. Q. Fan, Y. Kuang and F. T. Jiang, Konjac glucomannan-based nanocomposite spray coating with antimicrobial, gas barrier, UV blocking, and antioxidation for bananas preservation, *Int. J. Biol. Macromol.*, 2024, **265**, 130895, DOI: 10.1016/j.ijbiomac.2024.130895.

12 K. Ding, Y. Xie, H. S. Xu, S. Q. Xu, S. Ge, H. Li, X. Chang, J. N. Chen, R. R. Wang, Y. Shan and S. H. Ding, Visible light-responsive TiO_2-based hybrid nanofiller reinforced multifunctional chitosan film for effective fruit preservation, *Food Chem.*, 2024, **460**, 140539, DOI: 10.1016/j.foodchem.2024.140539.

13 W. Y. Sheng, L. Yang, Y. C. Yang, C. Z. Wang, G. Y. Jiang and Y. Q. Tian, Photo-responsive Cu-tannic acid nanoparticle-mediated antibacterial film for efficient preservation of strawberries, *Food Chem.*, 2025, **464**, 141711, DOI: 10.1016/j.foodchem.2024.141711.

14 C. M. Roberto and G. Boczkaj, Paving the way for green cross-linker substances for the fabrication of polymer membranes-a review, *Curr. Opin. Chem. Eng.*, 2025, **47**, 101097, DOI: 10.1016/j.coche.2025.101097.

15 X. X. Chang, N. M. Mubarak, S. A. Mazari, A. S. Jatoi, A. Ahmad, M. Khalid, R. Walvekar, E. C. Abdullah, R. R. Karri, M. T. H. Siddiqui and S. Nizamuddin, A review on the properties and applications of chitosan, cellulose and deep eutectic solvent in green chemistry, *J. Ind. Eng. Chem.*, 2021, **104**, 362–380, DOI: 10.1016/j.jiec.2021.08.033.

16 Y. Hu, P. Y. Liang, Z. X. Wang, C. P. Jiang, Q. F. Zeng, C. Y. Shen, Y. F. Wu, L. Liu, Y. K. Yi, H. X. Zhu and Q. Liu, Exploring the mechanism of solubilization and release of

isoliquiritigenin in deep eutectic solvents, *Int. J. Pharm.*, 2023, **644**, 123298, DOI: 10.1016/j.ijpharm.2023.123298.

17 J. H. Yu, S. L. Xu, R. H. Chen and P. Shao, A promising bioactive chitosan film in strawberry fresh-keeping: plasticized with tomato processing by-product extract of deep eutectic solvent, *Food Hydrocolloids*, 2024, **151**, 109859, DOI: 10.1016/j.foodhyd.2024.109859.

18 M. A. Smirnov, A. L. Nikolaeva, N. V. Bobrova, V. K. Vorobiov, A. V. Smirnov, E. Lahderanta and M. P. Sokolova, Self-healing films based on chitosan containing citric acid/choline chloride deep eutectic solvent, *Polym. Test.*, 2021, **97**, 107156, DOI: 10.1016/j.polymertesting.2021.107156.

19 W. Zhang, J. D. Shen, P. Gao, Q. X. Jiang and W. S. Xia, Sustainable chitosan films containing a betaine-based deep eutectic solvent and lignin: Physicochemical, antioxidant, and antimicrobial properties, *Food Hydrocolloids*, 2022, **129**, 107656, DOI: 10.1016/j.foodhyd.2022.107656.

20 T. Wahyono, D. A. Astuti, I. K. G. Wiryawan, I. Sugoro and A. Jayanegara, Fourier transform mid-infrared (FTIR) spectroscopy to identify tannin compounds in the panicle of sorghum mutant lines, *IOP Conf. Ser.:Mater. Sci. Eng.*, 2019, **546**, 042045, DOI: 10.1088/1757-899x/546/4/042045.

21 C. S. Jia, D. D. Cao, S. P. Ji, X. M. Zhang and B. Muhoza, Tannic acid-assisted cross-linked nanoparticles as a delivery system of eugenol: The characterization, thermal degradation and antioxidant properties, *Food Hydrocolloids*, 2020, **104**, 105717, DOI: 10.1016/j.foodhyd.2020.105717.

22 X. H. Hao, A. Shen, M. W. Li, R. C. Duan, L. L. Hou, X. Q. Zhao, Z. Q. Li, Y. W. Zhao, P. Q. Zhang, X. B. Wang, X. Li and Y. X. Yang, Simple method for visual detection of nitrite using fluorescence and colorimetry by poly (tannic acid) nanoparticles, *Anal. Chim. Acta*, 2023, **1263**, 341280, DOI: 10.1016/j.aca.2023.341280.

23 N. Sahiner, S. Sagbas, N. Aktas and C. Silan, Inherently antioxidant and antimicrobial tannic acid release from poly(tannic acid) nanoparticles with controllable degradability, *Colloids Surf., B*, 2016, **142**, 334–343, DOI: 10.1016/j.colsurfb.2016.03.006.

24 C. D. Qiao, X. G. Ma, X. J. Wang and L. B. Liu, Structure and properties of chitosan films: Effect of the type of solvent acid, *LWT–Food Sci. Technol.*, 2021, **135**, 109984, DOI: 10.1016/j.lwt.2020.109984.

25 S. Jiang, C. D. Qiao, R. P. Liu, Q. Z. Liu, J. Xu and J. S. Yao, Structure and properties of citric acid cross-linked chitosan/poly(vinyl alcohol) composite films for food packaging applications, *Carbohydr. Polym.*, 2023, **312**, 120842, DOI: 10.1016/j.carbpol.2023.120842.

26 H. J. Wu, Y. L. Lei, J. Y. Lu, R. Zhu, D. Xiao, C. Jiao, R. Xia, Z. Q. Zhang, G. H. Shen, Y. T. Liu, S. S. Li and M. L. Li, Effect of citric acid induced crosslinking on the structure and properties of potato starch/chitosan composite films, *Food Hydrocolloids*, 2019, **97**, 105208, DOI: 10.1016/j.foodhyd.2019.105208.

27 M. A. Smirnov, A. L. Nikolaeva, N. V. Bobrova, V. K. Vorobiov, A. V. Smirnov, E. Lahderanta and M. P. Sokolova, Self-healing films based on chitosan containing citric acid/choline chloride deep eutectic solvent, *Polym. Test.*, 2021, **97**, 107156, DOI: 10.1016/j.polymertesting.2021.107156.

28 Y. Zhao, R. Tian, Q. Zhang, L. Z. Jiang, J. Wang, Y. Zhang and X. N. Sui, Enhancing the properties of soy protein isolate and dialdehyde starch films for food packaging applications through tannic acid crosslinking, *Carbohydr. Polym.*, 2024, **332**, 121903, DOI: 10.1016/j.carbpol.2024.121903.

29 F. Xie, X. F. Feng, Z. J. Wang, D. Zhang, Q. Q. Chen, Z. J. He, S. Z. He, X. L. Wang, Y. S. Wu and J. Cai, Bioinspired starch nanofibrous films with tunable hydrophobicity and water adhesion via tannic acid-interfacial self-assembly for food packaging, *Chem. Eng. J.*, 2024, **496**, 154113, DOI: 10.1016/j.cej.2024.154113.

30 H. Y. Yu, Y. Wang, R. D. Wang, Y. Ge and L. Y. Wang, Tannic acid crosslinked chitosan/gelatin/SiO_2 biopolymer film with superhydrophobic, antioxidant and UV resistance properties for prematuring fruit packaging, *Int. J. Biol. Macromol.*, 2024, **275**, 133368, DOI: 10.1016/j.ijbiomac.2024.133368.

31 F. Seidi, M. K. Yazdi, M. Jouyandeh, S. Habibzadeh, M. T. Munir, H. Vahabi, B. Bagheri, N. Rabiee, P. Zarrintaj and M. R. Saeb, Crystalline polysaccharides: A review, *Carbohydr. Polym.*, 2022, **275**, 118624, DOI: 10.1016/j.carbpol.2021.118624.

32 P. Taheri, R. Jahanmardi, M. Koosha and S. Abdi, Physical, mechanical and wound healing properties of chitosan/gelatin blend films containing tannic acid and/or bacterial nanocellulose, *Int. J. Biol. Macromol.*, 2020, **154**, 421–432, DOI: 10.1016/j.ijbiomac.2020.03.114.

33 W. Zhang, Q. X. Jiang, J. D. Shen, P. Gao, D. W. Yu, Y. S. Xu and W. S. Xia, The role of organic acid structures in changes of physicochemical and antioxidant properties of crosslinked chitosan films, *Food Packag. Shelf Life*, 2022, **31**, 100792, DOI: 10.1016/j.fpsl.2021.100792.

34 S. J. Lee, M. A. Gwak, K. Chathuranga, J. S. Lee, J. Koo and W. H. Park, Multifunctional chitosan/tannic acid composite films with improved anti-UV, antioxidant, and antimicrobial properties for active food packaging, *Food Hydrocolloids*, 2023, **136**, 108249, DOI: 10.1016/j.foodhyd.2022.108249.

35 A. L. A. Halim, A. Kamari and E. Phillip, Chitosan, gelatin and methylcellulose films incorporated with tannic acid for food packaging, *Int. J. Biol. Macromol.*, 2018, **120**, 1119–1126, DOI: 10.1016/j.ijbiomac.2018.08.169.

36 T. Liu, M. Ma, A. Ali, Q. L. Liu, R. Bai, K. Zhang, Y. Guan, Y. L. Wang, J. Liu and H. G. Zhou, Self-assembled copper tannic acid nanoparticles: A powerful nano-bactericide by valence shift of copper, *Nano Today*, 2024, **54**, 102071, DOI: 10.1016/j.nantod.2023.102071.

37 R. Venkatesan, A. A. Vetcher, B. A. Al-Asbahi and S. C. Kim, Chitosan-based films blended with tannic acid and moringa oleifera for application in food packaging: the preservation of strawberries (fragaria ananassa), *Polym*, 2024, **16**, 937, DOI: 10.3390/polym16070937.

38 Z. A. Khan, M. Y. Wani, A. Ahmad, M. T. Basha, N. A. Aly and A. . A. Yakout, Multifunctional chitosan-cross linked-curcumin-tannic acid biocomposites disrupt quorum

sensing and biofilm formation in pathogenic bacteria, *Int. J. Biol. Macromol.*, 2024, **271**, 132719, DOI: 10.1016/j.ijbiomac.2024.132719.

39 C. Qiu, B. C. Chen, W. Q. Yin, D. J. McClements, Z. Y. Jin and H. Y. Ji, Effect of cinnamaldehyde-tannic acid-zinc acetate nanoparticles and aldehyde crosslinking on properties of chitosan films and their application for beef preservation, *Food Hydrocolloids*, 2025, **161**, 110881, DOI: 10.1016/j.foodhyd.2024.110881.

40 H. Y. Yu, Y. Wang, R. D. Wang, Y. Ge and L. Y. Wang, Tannic acid crosslinked chitosan/gelatin/SiO_2 biopolymer film with superhydrophobic, antioxidant and UV resistance properties for prematuring fruit packaging, *Int. J. Biol. Macromol.*, 2024, **275**, 133368, DOI: 10.1016/j.ijbiomac.2024.133368.

41 R. T. Qie, S. Z. Moghaddam and E. Thormann, Fully biobased adhesive from chitosan and tannic acid with high water resistance, *ACS Sustainable Chem. Eng.*, 2024, **12**(11), 4456–4463, DOI: 10.1021/acssuschemeng.3c07306.

42 Y. F. Xiao, Z. Y. Dai, Y. Wang, Z. J. Yan, Y. M. Xu, M. R. Wang, M. Lei, Q. M. Zhang and K. Qian, Liquid interference mitigation in capacitive sensors using Cassie-Baxter state based on superhydrophobic surfaces, *ACS Appl. Electron. Mater.*, 2025, **7**, 4287–4296, DOI: 10.1021/acsaelm.5c00453.

43 Y. Z. Zhang, X. L. Gu, Y. S. Wang, X. M. Xu and L. Zhang, Solution landscape of droplets on rough surfaces: wetting transition and directional transport, *Soft Matter*, 2025, **21**, 2729–2737, DOI: 10.1039/d4sm01372g.

44 N. Das, D. Sarkar, S. Sau, A. Ali, S. Mandal, S. Das, P. P. Ray and N. A. Hoque, Wenzel model motivated, superwettable micro-motiffed membrane for droplet-driven, real-time acid rain sensor via sequential contact electrification strategy, *Mater. Today Energy*, 2025, **48**, 101812, DOI: 10.1016/j.mtener.2025.101812.

45 K. Y. Shao, L. L. Zhang, Y. P. Zhong and D. Wang, MoS_2 QDs-decorated mesoporous polydopamine nanoparticle as a GSH responsive peroxidase-like nanozyme for effective antibacterial therapy, *Chem. Eng. J.*, 2025, **519**, 165645, DOI: 10.1016/j.cej.2025.165645.

46 C. Cui, C. Y. Shao, L. Meng and J. Yang, High-strength, self-adhesive, and strain-sensitive chitosan/poly(acrylic acid) double-network nanocomposite hydrogels fabricated by salt-soaking strategy for flexible sensors, *ACS Appl. Mater. Interfaces*, 2019, **11**(42), 39228–39237, DOI: 10.1021/acsami.9b15817.

47 C. Y. Shao, L. Meng, M. Wang, C. Cui, B. Wang, C. R. Han, F. Xu and J. Yang, Mimicking dynamic adhesiveness and strain-stiffening behavior of biological tissues in tough and self-healable cellulose nanocomposite hydrogels, *ACS Appl. Mater. Interfaces*, 2019, **11**(6), 5885–5895, DOI: 10.1021/acsami.8b21588.

48 C. Y. Shao, L. Meng, C. Cui and J. Yang, An integrated self-healable and robust conductive hydrogel for dynamically self-adhesive and highly conformable electronic skin, *J. Mater. Chem. C*, 2019, **7**, 15208–15218, DOI: 10.1039/c9tc05467g.

49 L. Meng, C. Y. Shao, C. Cui, F. Xu, J. D. Lei and J. Yang, Autonomous self-healing silk fibroin injectable hydrogels formed via surfactant-free hydrophobic association, *ACS Appl. Mater. Interfaces*, 2020, **12**(1), 1628–1639, DOI: 10.1021/acsami.9b19415.

50 W. L. Liu, S. Kang, Q. S. Zhang, S. Chen, Q. Yang and B. Yan, Self-assembly fabrication of chitosan-tannic acid/MXene composite film with excellent antibacterial and antioxidant properties for fruit preservation, *Food Chem.*, 2023, **410**, 135405, DOI: 10.1016/j.foodchem.2023.135405.